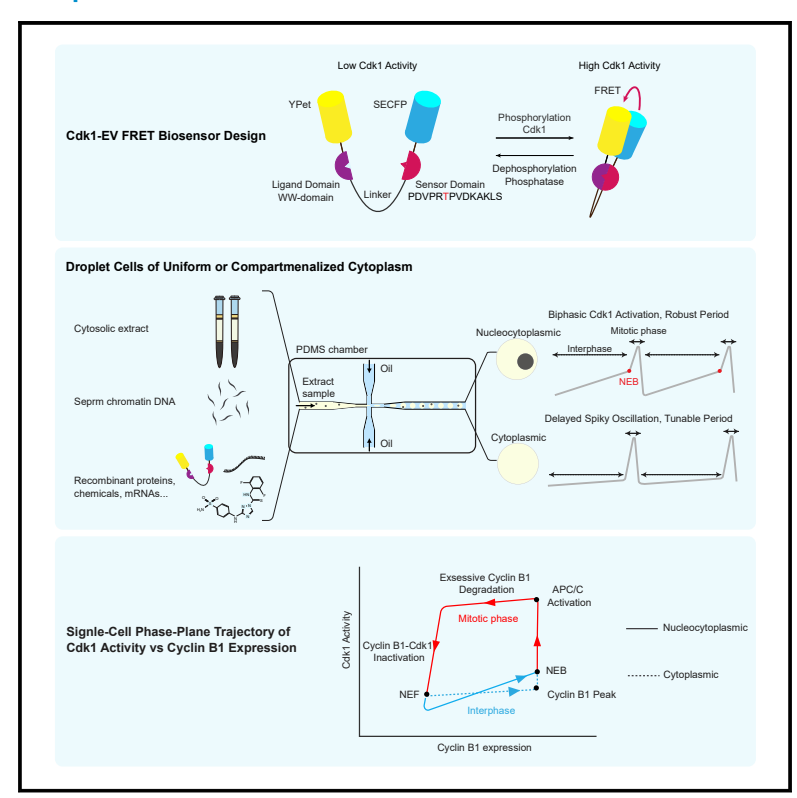
Nuclear-cytoplasmic compartmentalization of cyclin B1-Cdk1 promotes robust timing of mitotic events

Graphical abstract



Authors

Gembu Maryu, Qiong Yang

Correspondence qiongy@umich.edu

In brief

Compartmentalization, a ubiquitous feature of eukaryotic cells, provides spatiotemporal segregation to ensure faithful cellular processes. Maryu and Yang show that compared with a homogeneous microenvironment, nucleocytoplasmic compartmentalization of a mitotic master regulator Cdk1 significantly changes its activation profile, enhances clock robustness, and ensures correct order of downstream mitotic events.

Highlights

- Cdk1-EV tracks single-cell Cdk1 spatiotemporal dynamics for phase-plane orbit
- Compartmentalized Cdk1 turns a delayed bistable switch into biphasic activation
- Tunable Cdk1 clock in homogeneous cytosol becomes robust when nuclei are present
- Scalable degradation allows robust mitosis despite noisy cyclin B1 levels







Article

Nuclear-cytoplasmic compartmentalization of cyclin B1-Cdk1 promotes robust timing of mitotic events

Gembu Maryu¹ and Qiong Yang^{1,2,3,*}

- ¹Department of Biophysics, University of Michigan, Ann Arbor, MI 48109, USA
- ²Department of Physics, University of Michigan, Ann Arbor, MI 48109, USA
- 3Lead contact

*Correspondence: qiongy@umich.edu https://doi.org/10.1016/j.celrep.2022.111870

SUMMARY

The cyclin-dependent kinase (Cdk1) oscillator is widely characterized in homogenized cytosolic extracts, leaving unclear the impact of nucleocytoplasmic compartmentalization. Here, by developing a Förster resonance energy transfer (FRET) biosensor, we track Cdk1 spatiotemporal dynamics in reconstituted cells with or without side by side and find compartmentalization significantly modulates clock properties previously found in bulk studies. Although nucleus-absent cells display highly tunable frequency, the nucleus-present cells maintain constant frequency against cyclin B1 variations. Despite high expression variability, cyclin degraded within the same duration, enabling a robust mitotic phase. Moreover, Cdk1 and cyclin B1 cycle rigorously out-of-phase, ensuring wide phase-plane orbits, essential for oscillation robustness. Although Cdk1 in homogeneous extracts is well known for delayed switch-like activation, we find active cyclin B1-Cdk1 accumulates in nuclei, without delay, until the nuclear envelope breakdown (NEB) when another abrupt activation triggers anaphase. Cdk1 biphasic activation and spatial compartmentalization may together coordinate the accurate ordering of different downstream events.

INTRODUCTION

Mitosis of eukaryotes is regulated by a protein network centered on the cyclin B1-Cdk1 complex. In recent decades, studies applying well-mixed egg extracts from Xenopus laevis have contributed substantially to understanding how this network functions faithfully in driving the cell cycle into and out of mitosis.1 The entry of mitosis is triggered by a hysteretic switch-like activation of cyclin B1-Cdk1 that is regulated by the Cdk1/Wee1/Cdc25 interlinked positive feedback loops.²⁻⁵ This, in turn, activates the Cdk1 repressor, anaphase-promoting complex or cyclosome (APC/C), an E3 ubiquitin ligase that facilitates the degradation of cyclin B1 and inactivation of Cdk1, completing an essential negative feedback loop and leading to mitotic exit.⁶ Such positive-plus-negative feedback architecture has been computationally shown to function as a relaxation-type oscillator and can enhance robustness compared with a simple negative feedback design.^{7–12}

In addition to the positive feedback-driven hysteretic activation of Cdk1, phase shifts between the cyclin B1 synthesis-degradation cycle and Cdk1 activation-deactivation cycle are also important to sustain robust oscillations. In computational studies, both hysteresis and phase shifts ensure a large loop in the phase plane of active Cdk1 and cyclin B1 abundance, rather than superimposed upstroke and downstroke. 11,12 Thus, the shape of the phase-plane trajectory is crucial for understanding

the dynamical properties of the system. Bulk extract assays previously showed a wide triangle-shaped phase-plane orbit of cyclin and Cdk1 activity. However, these ensemble-averaged measurements for only one cycle may not precisely recapitulate the real-time cyclin and Cdk1 relationship in individuals.

Moreover, frequency and amplitude are functionally essential properties of biological oscillators. Although it is hard for a single negative feedback loop (e.g., Goodwin oscillator)¹³ to vary frequency without affecting its amplitude, theoretical studies suggested positive feedback can allow a broad frequency tuning decoupled from the amplitude, a phenomenon called frequency tunability that seems to share among various oscillators like heartbeats and neuronal spiking.¹² Although the Cdk1 network, featuring coupled positive and negative feedback, is predicted to exhibit frequency tunability, there has been no measurement to date to confirm it.

These features of the Cdk1 circuit have been characterized mainly using bulk experiments or modeling considering only spatially homogeneous conditions. However, many subcellular processes in eukaryotes are compartmentalized in membrane-bound nuclei and organelles, to increase their efficiency and specificity. Recent studies have identified spatial positive feedback that drives abrupt cyclin B1-Cdk1 nuclear translocation upon activation, 14,15 raising the question of whether the clock properties revealed in homogenized cytoplasmic extracts still hold in cells containing nuclei.





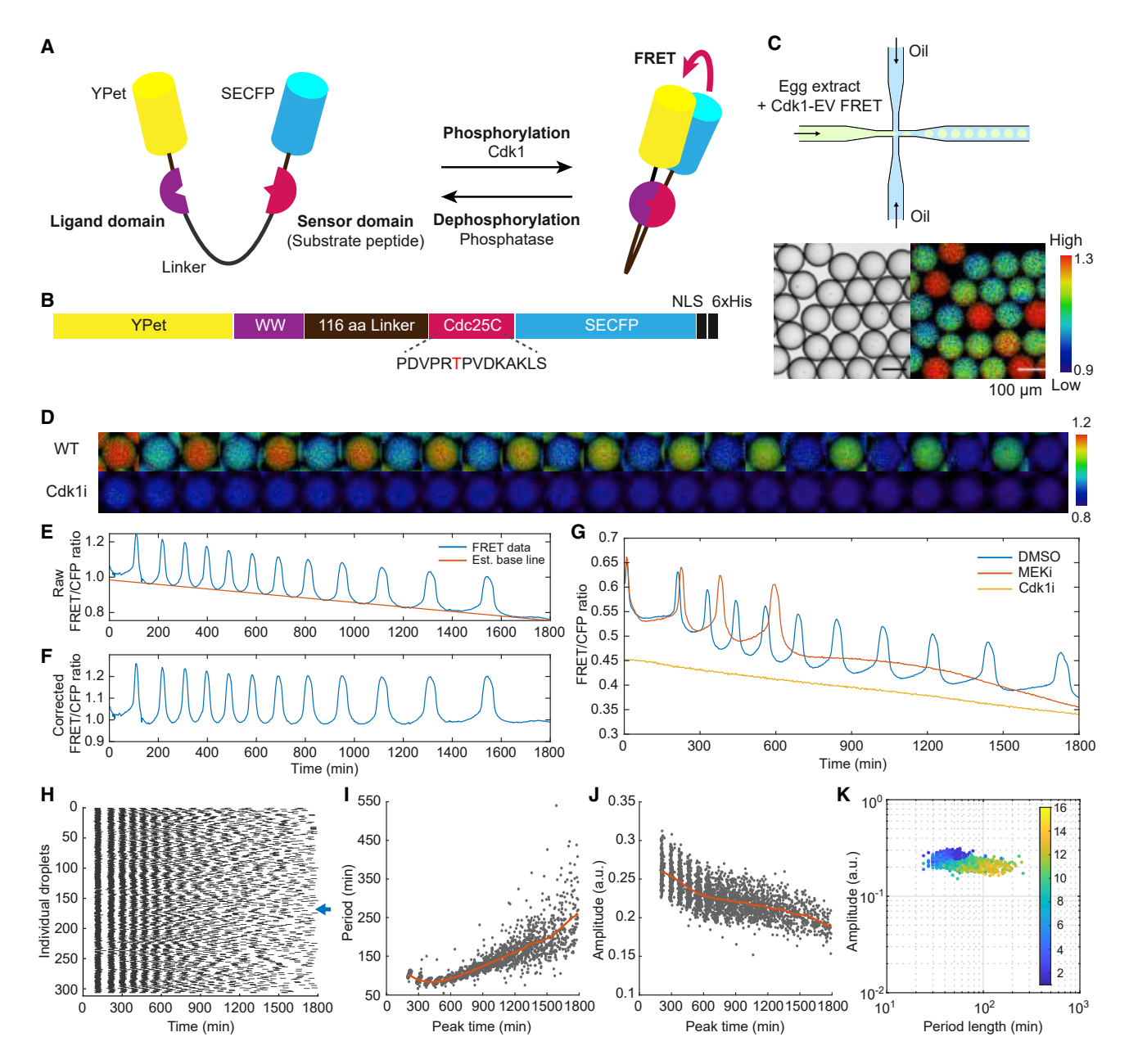


Figure 1. Cdk1-EV detects Cdk1 kinase activity specifically in droplet cells

(A) Scheme of Cdk1-EV FRET biosensor. FRET efficiency reversibly increases or decreases via phosphorylation by Cdk1 and dephosphorylation by antagonistic

- (B) The modified substrate sequence has a threonine phosphorylation site (red) by Cdk1. C terminus histidine tag is for protein purification.
- (C) Top: fluorosurfactant-stabilized droplets containing extracts and Cdk1-EV protein were formed on a microfluidic device with fluorinated oil. Bottom: a brightfield image was used for droplet segmentation. An emission ratio image was shown in the intensity-modulated display (IMD) mode. Color bar represents low (blue) to high (red) Cdk1 activity. Scale bar: 100 μm .
- (D) Representative droplets from positive control (wild-type [WT]; top), showing 12 cycles of FRET peaks (mitotic phase) and troughs (interphase), and 1 µM Cdk1/ 2 inhibitor III treated condition (Cdk1i; bottom); images selected at the same frame as WT.
- (E) Raw emission ratio time course of WT droplet in (D) (blue). Baseline was estimated by troughs of FRET oscillations (red).
- (F) Same as (E) after baseline correction. Corrected data were used to quantify the oscillation amplitude in later analyses.
- (G) Time courses of representative droplets treated with 1 μ M MEK inhibitor PD0325901 (red), 1 μ M Cdk1 inhibitor Cdk1/2 inhibitor III (yellow), and DMSO (blue) as a control.

(legend continued on next page)

Article



Here, to explore the impact of nucleocytoplasmic compartmentalization, we reconstituted the Cdk1 circuit in water-in-oil microemulsion droplets that contain either the homogenized Xenopus egg cytoplasm or cytoplasm supplied with demembranated sperm chromatin to induce spontaneous nuclear formation. We also developed a Förster (or fluorescence) resonance energy transfer (FRET) biosensor for long-term timelapse imaging of Cdk1 spatiotemporal dynamics in these droplet cells. We first investigated the amplitude-to-frequency response in cytoplasmic cells and found them highly tunable in frequency without changing the amplitude. However, the clock frequency became robust against cyclin variations in nucleus-present cells, suggesting a possible buffering mechanism of the nucleus compartment. The presence of nuclei also changed the Cdk1 activation profile from a simple off-to-on switch into a two-phase activation, including a gradual nuclear cyclin B1-Cdk1 accumulation before nuclear envelope breakdown (NEB) and a sharp cyclin-independent switch after NEB. The two-step activation in combination with spatial segregation may ensure the correct order of mitotic events. Using fluorescence-tagged cyclins and FRET, we also simultaneously tracked cyclin B1 expression and Cdk1 activity in single droplets for multiple cycles, revealing their dynamical relationship in real-time phase-plane trajectories. These measurements provided a detailed picture of the correlation between cyclin and Cdk1 cycles and the downstream nuclear events at the single-cell level.

RESULTS

EKAREV FRET biosensor was modified for cyclin B1-Cdk1 activity monitoring

To visualize Cdk1 kinase activity in both spatially homogeneous and heterogeneous conditions, we sought to implement a FRET biosensor in Xenopus extracts. A Cdk1 FRET biosensor was previously developed based on a polo-box domain (PBD) of Plk1 as the phospho-binding domain and the autophosphorylation site from human cyclin B1 and applied in mammalian cells^{16,17} and *Drosophila* embryos.¹⁸ However, it did not perform well in our Xenopus system (Figure S1B). To design a new Cdk1 sensor with an improved signal-to-noise ratio, we modified a substrate sequence of an existing ERK FRET biosensor known as EKAREV. 19,20 The resulting sensor (hereafter named Cdk1-EV) includes a donor-acceptor fluorescent protein pair with optimized energy transfer efficiency (SECFP and YPet), sequence from Cdc25C as a consensus phosphorylation site for Cdk1 in the mitotic phase²¹⁻²³ (sensor domain), the WW domain known as the phosphopeptide binding domain (ligand domain), and a flexible 116 amino acid EV linker (Figure 1A). ERK-specific binding sequence FQFP peptide is further removed to improve the specificity for Cdk1 (Figure 1B). Upon Cdk1 activation, the

phosphorylated sensor domain is bound by the ligand domain, thereby inducing a conformational change that alters the FRET efficiency between fluorescent proteins, which can be quantified by calculating ratio values of the donor-to-acceptor emission fluorescence intensities.

The biosensor is specific to cyclin B1-Cdk1 kinase activity

To test the Cdk1-EV FRET biosensor, we purified the protein by bacterial overexpression system to apply to Xenopus cycling egg extracts before encapsulating them in cell-sized microemulsion droplets via a microfluidic device (Figure 1C).²⁴⁻²⁶ We observed that the FRET/cyan fluorescent protein (CFP) emission ratio changed periodically in each droplet (Figure 1D, top row; Figure 1E, blue; Video S1) despite an overall decay of the baseline (Figure 1E, red). The baseline decay was likely caused by photobleaching rather than some intrinsic signal reduction, as it was also seen in the phospho-dead TA mutant (Figure S1A, red) and under Cdk1 inhibitor-treated condition (Figure 1G, yellow). After baseline correction, the FRET/CFP ratio reports 12 undamped, self-sustained oscillations between active and inactive states of Cdk1 (Figure 1F). The emission ratio from trough to peak of Cdk1-EV was greater than 20%, better than the reported values for the Plk1-cyclin B1-based Cdk1 FRET sensor in mammalian cells $(10\%-15\%)^{16}$ and *Drosophila* embryos (6%). 18 We also compared the two sensors side by side in our cell-free system prepared from the same batch of eggs. Although Cdk1-EV reported clear oscillations (Figures S1B and S1C, blue), the Plk1-cyclin B1-based sensor, either with its original linker (Figure S1B, red) or with the linker replaced by a long, flexible EV linker (Figure S1C, red), could barely detect the signal. These extracts themselves were oscillatory as their reconstituted nuclei could undergo periodic nuclear envelope breakdown and reformation, as indicated by a nuclear marker, protein of nuclear localization signal (NLS) fused with mCherry, NLS-mCherry-NLS (Figures S1A-S1C, right panels).

To demonstrate Cdk1-EV responds only to Cdk1 activity, we treated the same extracts with DMSO (positive control), 1 μ M Cdk1/2 inhibitor III (CAS 443798-55-8), or 1 μM PD0325901 MEK inhibitor before encapsulation. In contrast to oscillations observed in the DMSO control (Figure 1G, blue), the emission ratio in the Cdk1-inhibited droplets was completely suppressed to a constantly low level, as expected (Figure 1D, bottom row; Figure 1G, yellow). MEK inhibition did not terminate oscillations; however, compared with the DMSO control, it elongated the cell cycle periods and reduced the number of cycles (Figure 1G, red), possibly because ERK is one of the pivotal kinases for cell cycle progression.²⁷ Moreover, we did not observe spontaneous ratio changes in interphase as EKAREV reported in human culture cells.^{21,28} These results indicate Cdk1-EV specifically measures the Cdk1 activity with higher sensitivity than the previously reported sensor.

⁽H) Raster plot of FRET/CFP ratio peak times for 307 droplets. The droplets were initially synchronized and dephased over cycles. The blue arrow indicates the representative droplet shown in (D)-(F).

⁽I and J) Period (I) and amplitude (J) of Cdk1 oscillations. The trend was shown by kernel density estimation (red).

⁽K) The fold change of period length was greater than amplitude. Color bar represents the cycle number. See also Figure S1 and Video S1.





Cell cycle behaves as a period-tunable, amplitudeconstant oscillator in homogenized cytoplasm

With this sensor, we first examined the Cdk1 amplitude-frequency dependency in cytoplasmic-only droplets. Oscillations initially synchronized among individual droplets were gradually dephased over the cycles (Figure 1H), possibly contributed by both the partitioning effects during encapsulation^{29,30} and random phase fluctuations.³¹ The oscillation period elongated significantly from roughly 50 to 300 min (Figure 1I), while the amplitude of FRET remained relatively constant, decreased slightly from 0.3 to less than 0.2 throughout the experiment spanning 30 h (Figure 1J). What causes the period elongation is still unknown, but we could previously explain the observation using an energy depletion model.²⁴ The trend is better visualized in an amplitude-period log-log plot (Figure 1K), showing a significantly greater fold change in period than amplitude.

To explicitly tune the frequency and measure the amplitudeto-period response, we systematically perturbed the endogenous cyclin B mRNA translation using morpholinos (MOs), antisense oligonucleotides against the isoforms of Xenopus cyclin B1/B2 mRNA species. We co-injected the MOs and purified blue fluorescent protein (BFP) as the MOs concentration indicator into one inlet of a two-channel tuning microfluidic device before extract encapsulation, creating a broad spectrum of MOs concentrations across the droplets (Figure 2A). These droplet cells showed MOs-dependent oscillations (Figure 2B), with fewer cycles (Figure 2C), steadily increased rising periods (Figure 2D, blue), and stable falling periods (Figure 2D, red) for increased MOs concentrations. However, both rising and falling amplitudes were almost uniform across a broad range of MOs concentrations (Figure 2E). The amplitude-period relation had zero slope, with invariant amplitude versus a widely changed period with the MOs concentration (color coded by the BFP intensity) (Figure 2F), indicating the frequency tuning is decoupled from the amplitude.

We also tuned up the speed by adding human cyclin B1-Katushka mRNAs (0, 10, 25, and 50 ng/µL) to the MO-treated extracts that silenced endogenous Xenopus cyclins and found the Cdk1 activity waveform is closely dependent on the exogenous mRNA concentration (Figure 2G). With increased human cyclin B1-Katushka mRNA concentration, we observed cycle numbers increased (Figure 2H), rising periods decreased (Figure 2I, blue), and falling periods unvaried (Figure 2I, red). The amplitude was kept within a similar range across different mRNA concentrations (Figure 2J), resulting in a flat amplitudeperiod dependency (Figure 2K). Excessive MOs (Figure S2A, red) or mRNA (Figure S2A, blue) outside the dynamic range will arrest Cdk1 at a stable steady state, inactive (emission ratio < 1) or active (emission ratio > 1.2) respectively.

Together, cytoplasmic cells displayed consistent clock behaviors across all different experimental conditions (e.g., highly tunable interphase, robust mitotic duration, and constant Cdk1 amplitude). These intrinsic properties are theoretically associated with the Cdk1 coupled positive and negative feedback topology. 12 Our amplitude-period measurements provide the first explicit experimental evidence for this long speculated behavior.

Nuclear-cytoplasmic compartmentalization promotes robust mitotic timing

To understand the impact of cellular compartmentalization, we added demembranated sperm chromatin into cycling extracts before encapsulation to induce the self-assembly of nuclei. Because of random encapsulation following Poisson statistics, droplets prepared from the same bulk may or may not contain a nucleus, detectable by NLS-mCherry-NLS nuclear marker, providing a unique system for tracking the clock dynamics in the presence or absence of nuclei in parallel (Figure 3A; Video S2). As activated cyclin B1-Cdk1 translocates into the nucleus rapidly and irreversibly until NEB, 14,15 we also tagged the FRET biosensor by NLS to visualize nuclear-specific Cdk1 activation efficiently. In both droplets with and without a nucleus, we observed Cdk1 oscillations with period elongation over time (Figure 3B). The nuclear droplet showed a significantly shorter period in initial cycles than the cytoplasmic droplet (Figure 3C), possibly explained by the abrupt translocation of active cyclin B1-Cdk1 into the nucleus to effectively increase its concentration and accelerate the mitotic entry.

Intriguingly, while oscillations easily speed up with exogenous cyclin mRNAs in the nucleus-free cells (Figure 3D, gray; Figure 3E, columns 2, 4, 6, and 8), a frequency-tunability phenomenon as observed before, we found the system hardly reacts to the cyclin increase and maintains an almost constant period when a nucleus is present (Figure 3D, blue; Figure 3E, columns 1, 3, 5, and 7).

Nuclear-cytoplasmic compartmentalization facilitates biphasic activation of Cdk1 and temporal ordering of mitotic events

We also found that the oscillation profiles are qualitatively different between droplets with or without a nucleus. Cdk1 in cytoplasmic droplets remained inactive throughout the interphase before a sharp activation at mitosis. This delayed, spikeshaped Cdk1 activation is well described in cell cycle models considering no spatial variability (Figures 3B and 3D, gray).^{6,32} However, in nucleocytoplasmic droplets, Cdk1 steadily increased, from the beginning of interphase, to a moderate activity before a quick jump to a distinctively higher activity (Figures 3B and 3D, blue).

To examine whether this biphasic activation of Cdk1 may correlate with any of the downstream mitotic events, we developed an algorithm to automatically segment the nucleus and extracted the time of nuclear envelope formation (NEF) (blue dot), NEB start (green dot), and NEB end (red dot) on the basis of the cytoplasmic/nuclear (C/N) ratio (Figure 3F, orange) and SD (Figure 3F, gray) of NLS-mCherry-NLS (STAR Methods; Figures S3A-S3C). We found NEF started before Cdk1 was fully inactivated, and the turning point of the biphasic Cdk1 activation coincided with NEB end (Figures 3G and S3D). Aligning all individual cycles to their FRET/CFP ratio at NEF showed clearly Cdk1 undershoots after NEF (Figure S3E, blue dots). Aligning these curves at peak time, we found a relatively uniform Cdk1 inactivation phase (from Cdk1 peak to trough), although the duration and steepness of its interphase activation (from Cdk1 trough to NEB) are highly varied, likely caused by the cyclin mRNA variation (Figure 3H). Yet despite the interphase

Article



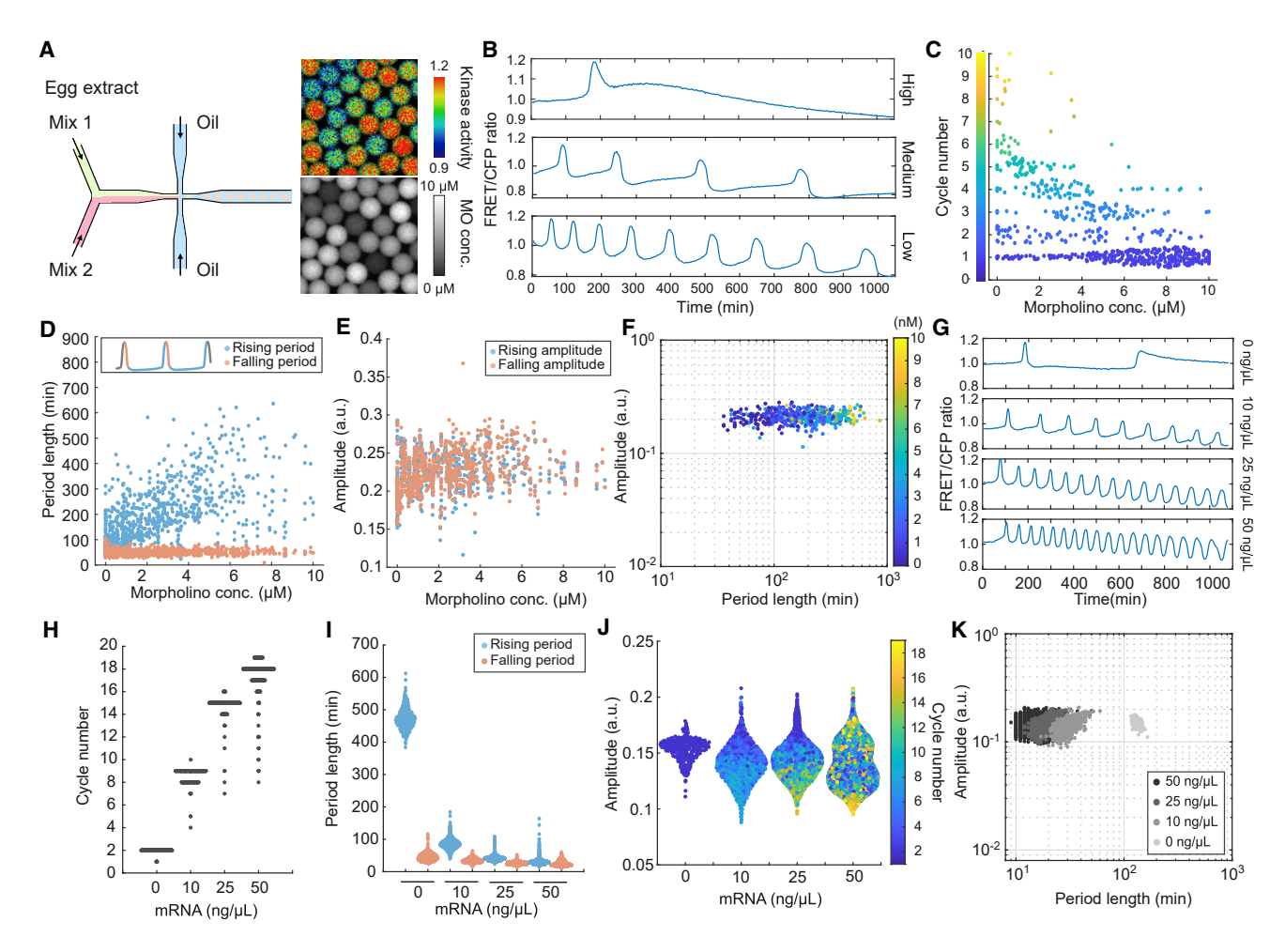


Figure 2. Cdk1-EV in homogeneous cytoplasm reveals cell cycle period tunability

(A) Left: scheme of two-channel tuning. Mix 1 (extracts plus Cdk1-EV) and mix 2 (mix 1 plus 10 μM MOs plus recombinant BFP as MOs concentration indicator) were encapsulated into droplets at different ratios. Right: FRET and BFP intensity of representative droplets were shown in IMD mode and grayscale images. (B) Representative Cdk1 oscillation raw-data profiles from different MOs concentrations (low, medium, and high).

(C) The distribution of the total cycle number of individual droplets was changed with MOs concentration (determined by BFP intensity). The maximum total cycle number decreases with MOs concentration.

(D) Rising period (the time from a trough to the next peak; blue) and falling period (the time from a peak to the next trough; red) of Cdk1 oscillation versus MOs concentration. Each dot indicates an individual cycle of the first 4 cycles.

(E and F) used the same criteria. (E) Rising amplitudes (blue) and falling amplitudes (red) versus MOs concentration. (F) Log-log plot of amplitude (calculated as the average of rising amplitude and falling amplitude) and period. Color bar represents MOs concentration.

(G) Raw FRET/CFP ratio time courses of representative droplets treated with 10 µM Xenopus cyclin B MOs and various amounts of manually added exogenous human cyclin B1-Katushka mRNA. Cdk1 oscillation suppressed by MOs was recovered by mRNA. (G)-(K) use the same data.

(H–J) Column scatterplots of cycle number (H), period (I), and amplitude (J) at different mRNA concentrations. Each dot in (H) represents the total cycle number of a single droplet. Each dot in (I) and (J) represents an individual cycle of a single droplet. Color bar in (J) represents the cycle number.

(K) Amplitude-period log-log plot for clusters of droplets with different mRNA concentrations. See also Figure S2.

variability, by aligning all curves on the basis of their Cdk1 trough values, we observed a robust threshold of Cdk1 activity at NEB end, beyond which the abrupt second-phase activation is triggered (Figure S3F, red dots). Unlike the fluctuating speed of Cdk1 first-phase activation, the steepness of its second-phase activation was consistent across all droplets and collapsed into one line after aligning all curves at NEB end (Figure 3I). The second-phase activation only spanned a brief period (10-15 min regardless of the interphase length), likely controlled by the hysteresis switch. It may also be contributed by active cytoplasmic Cdk1 accessible to NLS-tagged FRET sensors upon NEB.¹⁵ For either mechanism or a combination of both, the distinct two phases of activation may ensure the segregation of early and late mitotic events.

To summarize the main features of Cdk1 activation affected by compartmentalization, we standardized all data into 250 datapoint arrays (Figure 3J; STAR Methods). Without a nucleus, Cdk1 remains a constant basal level throughput interphase



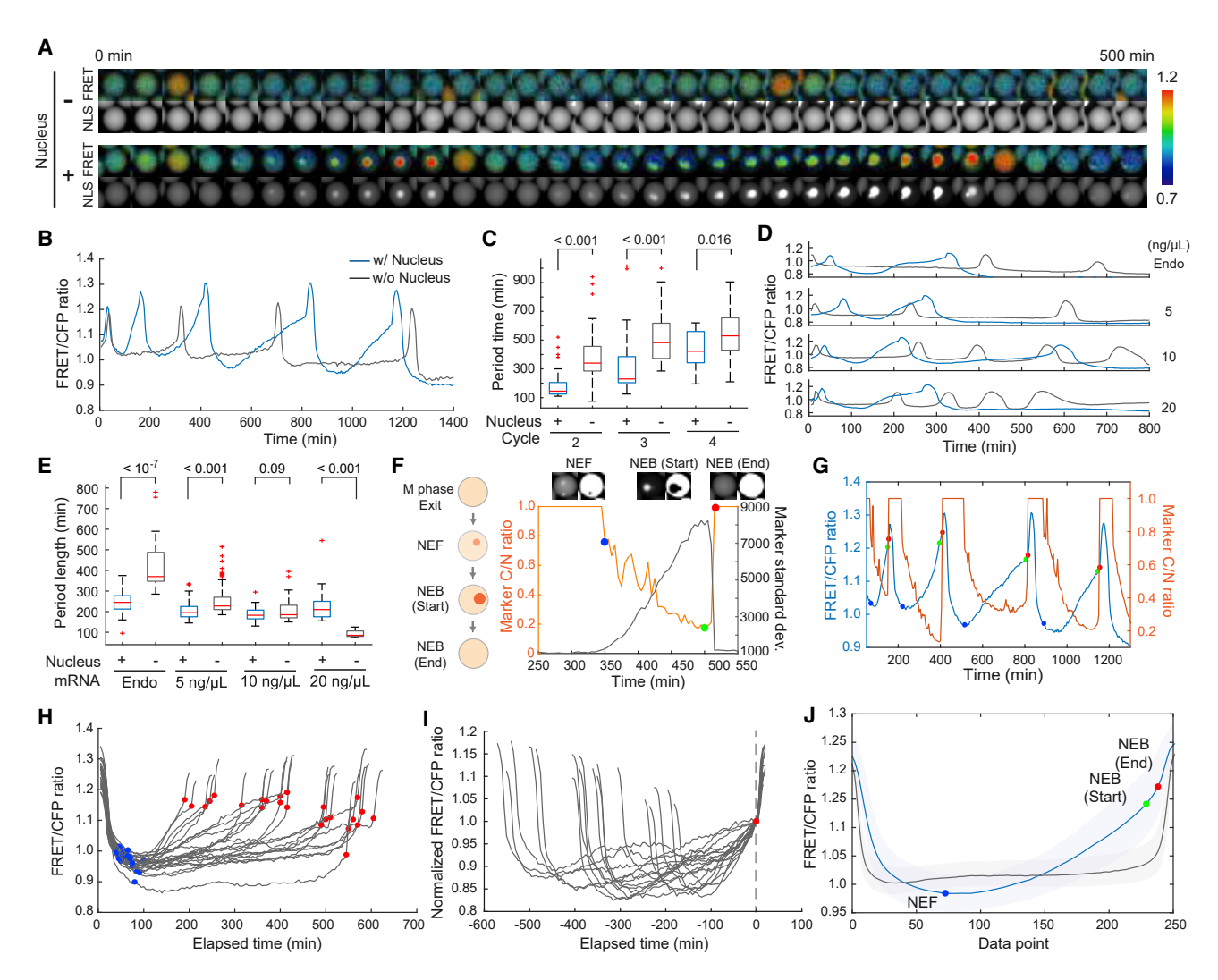


Figure 3. Nuclear compartmentalization affects the Cdk1 activation profile and period tunability

(A) A representative droplet having a nucleus (+; rows 3 and 4) or not (-; rows 1 and 2). Cdk1 activity was shown in IMD images (rows 1 and 3). NLS-mCherry-NLS is for detecting nuclei (rows 2 and 4).

(B) Cdk1 activity time courses for droplets in (A), showing single spiky activations for the droplet without nucleus (gray) versus biphasic activations for the droplet with nucleus (blue). FRET/CFP ratio value was normalized by dividing by the average of 1st trough values of cytoplasmic droplets. The same normalization method applied to (G), (H), and (J).

(C) Boxplot of period of individual cycles in droplets with (+) or without (-) nuclei. The period is calculated on the basis of the peak-to-peak time. Cycle 2: 1st to 2nd peak, (+) n = 75, (-) n = 55; cycle 3: 2nd to 3rd peak, (+) n = 54, (-) n = 40; cycle 4: 3rd to 4th peak, (+) n = 24, (-) n = 22. Later cycles had longer period durations. p values in (C) and (E) were calculated using two-sample t tests.

(D and E) Raw Cdk1 activity time courses of representative droplets (D) and boxplot of first periods for all droplets (E) with (blue) or without (gray) nuclei. Extracts were supplied with 0 (endogenous), 5, 10, and 20 ng/μL cyclin B1-Katushka mRNA. Cytoplasmic droplets oscillate faster with mRNA additions, but nucleocytoplasmic droplets remained a constant speed. Also, a small jump just before the peak was observed in nucleocytoplasmic droplets as seen in (B). Sample size in (E): endo (+) n = 33, (-) = 20; 5 $ng/\mu L$ (+) n = 93, (-) = 160; 10 $ng/\mu L$ (+) n = 28, (-) = 53; 20 $ng/\mu L$ (+) n = 33, (-) n = 21.

(F) Time courses of cytoplasmic/nuclear (C/N) ratio (gray) and SD (orange) of a nuclear marker, NLS-mCherry-NLS, over one cycle. The nuclear marker SD and the skewness of the marker intensity histogram (Figure S3A) were used to segment the nuclear region (binary images), which was used to calculate C/N. C/N = 1.0 indicates no nucleus. With this value, the time points of NEF (blue), NEB start (green), and NEB end (red) were determined.

(G) Time courses of the nuclear marker C/N ratio (orange) and Cdk1 activity (blue line) with defined nuclear events (NEF, blue dot; NEB start, green dot; NEB end,

(H) Cdk1 activity cycles were aligned at the left peak time, with NEF (blue dot) and NEB end (red dot) marked on each cycle.

(I) The curves in (H) were aligned and normalized at NEB end (red dot, vertical gray dotted line). The steepness of the ratio change after NEB end was similar among droplets.

(J) Cdk1 activities of all cytoplasmic (gray; n = 121) and nucleocytoplasmic (blue; n = 162) droplets were transformed into 250 datapoint arrays and their mean and SD values were plotted as solid line and shade. The time information of nuclear events was also transformed and plotted with the nucleocytoplasmic curve. See also Figure S3 and Video S2.



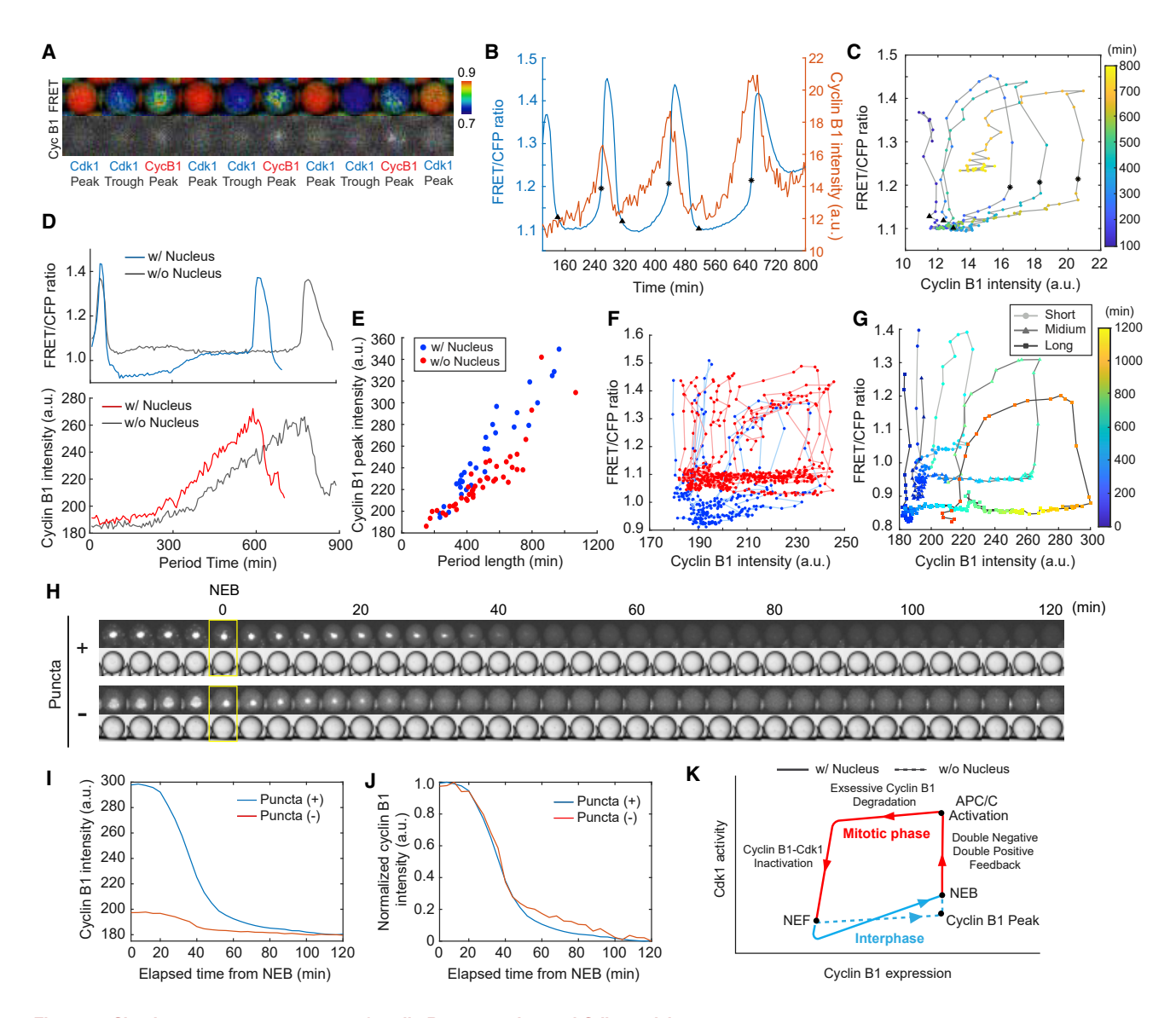


Figure 4. Simultaneous measurements of cyclin B1 expression and Cdk1 activity

(A) Cdk1 FRET/CFP ratio IMD images and cyclin B1-mScarlet-i fluorescent images at Cdk1 peaks, Cdk1 troughs, and cyclin B1 peaks for a representative droplet. There was a time gap between the peaks of Cdk1 and cyclin B1. This droplet was treated with 10 μM MOs and 50 ng/μL cyclin B1-mScarlet-i mRNA. Bright spots in the cyclin B1 channel colocalized with those in the NLS-tagged Cdk1-EV channel.

- (B) Both Cdk1 activity (blue) with NEF (triangle) and NEB end (asterisk) and cyclin B1-mScarlet-i expression (red) were quantified simultaneously for multiple cycles. FRET ratio was baseline-corrected as in Figure 1 and was further normalized by dividing by the average of 1st trough values of cytoplasm-only droplets. Data were processed the same way in (D), (F), and (G).
- (C) Data in (B) were plotted as a phase-plane trajectory with NEF (triangle) and NEB end (asterisk) marked. Color bar indicates elapsed time from experiment start. The phase-plane orbits shift to the right over time.
- (D) Time courses of FRET and cyclin B1-Katushka in representative droplets that had a similar cyclin B1-Katushka expression level (both with Xenopus cyclin MOs plus 10 ng/µL human cyclin B1 mRNA). The period length of the nuclear droplet (blue in upper panel, red in lower panel) was shorter than the cytoplasmic droplet
- (E) Scatterplot of period and maximum intensity of cyclin B1 expression for droplets with (blue) and without (red) nucleus. Nuclear droplets had shorter periods than cytoplasmic droplets that have similar cyclin B1 expression levels, as also observed in Figure 3C.
- (F) The shapes of phase-plane orbits were compared between spatially homogeneous and heterogeneous cellular environments. Branch #1 of nucleocytoplasmic droplets (blue) started lower than that of cytoplasmic droplets (red), as described in Figure 3J. The path of Cdk1 activation after NEB and cyclin B1-Cdk1 inactivation were not different between conditions.
- (G) Representative phase-plane orbits of different period lengths were plotted for droplets with a nucleus. Phase-plane orbits shifted right and became wider as period length increased. A plateau high Cdk1 activity was observed (branch #3) in the long period orbit.





before a burst-like activation (gray). With a nucleus, following a deeper deactivation after NEF, Cdk1 undergoes gradual interphase activation and a steeper second-phase activation separated by NEB end (blue).

High-resolution mapping of mitotic events on single-cell phase-plane trajectories

To obtain a complete picture of the Cdk1 activation-deactivation cycle in relation to the cyclin synthesis-degradation cycle and their relationships with the downstream nuclear events, we performed a long-term single-cell tracking of Cdk1 activity and total cyclin B1 (Figures 4A-4C). Cdk1 activity is measured by the Cdk1-EV, as described before; to simultaneously measure the total cyclin B1 level over time in the same droplet, we co-applied the mRNA of cyclin B1 tagged with a fluorescent protein (cyclin B1-FP) before droplet encapsulation and imaging. Cyclin B1-FP (cyclin B1-mScarlet-i or cyclin B1-Katushka used interchangeably in this study) is synthesized during interphase and ubiquitinated for degradation by the APC/C upon metaphase-anaphase transition.

In an example droplet containing Cdk1-EV and mRNA of human cyclin B1-mScarlet-i (Figure 4A; Video S3), we show colocalization of Cdk1 FRET and cyclin B1-mScarlet-i signals inside the nucleus until NEB, consistent with the observations of nuclear localization of cyclin B1-Cdk1 in late G2 of mammalian cells. 14,15 But in mammalian cells, cyclin was in the cytoplasm until late G2, while we do not observe any enriched cytoplasmic cyclins as the rapid early embryonic cycles skip the G1/G2 gap phases. The peaks and troughs of cyclin B1 were clearly out of phase with Cdk1 activity (Figure 4B), producing a phase-plane trajectory that featured three cycles of wide, square-shaped loops, each containing four branches in temporal orders (Figure 4C): an interphase Cdk1 activation, rate limited by cyclin synthesis (branch #1, bottom horizontal); an abrupt Cdk1 activation independent of cyclin (branch #2, right vertical); degradation of cyclin B1 during which Cdk1 changed a little (branch #3, top horizontal); and a fast Cdk1 inactivation (branch #4, left vertical). The progression time required to pass each phase (estimated by the number of datapoints of 4-min interval) suggests interphase (branch #1) is the slowest and mitotic phases are fast (branches #2-4). We also mapped NEF (Figures 4B and 4C, triangles) and NEB end (Figures 4B and 4C, asterisks) on the orbits to obtain an accurate temporal correlation of key mitotic events with cyclin and Cdk1 dynamics. On each cycle, cyclin B1 peaked at the end of Cdk1 first-phase activation, right before NEB end, but the degradation of cyclin B1 was not detectable until the Cdk1's second activation was complete, suggesting the APC/C activation and anaphase onset require higher Cdk1 activity. NEF happened when Cdk1 activity dropped below a threshold lower than the threshold for NEB; Cdk1 inactivation continued even after NEF

initiated and cyclin started to re-accumulate, an undershootlike phenomenon revealed by high-resolution mapping (Figures 3G, S3E, and 4C).

As a rate-limiting factor for Cdk1 activation, cyclin B1 at a slower synthesis rate usually produces longer interphase. However, we observed period elongation even the cyclin B1 synthesis rate did not decrease, resulting in increased cyclin B1 peak expression (Figure 4B, red) and right-shifted phase-plane orbit each cycle (Figure 4C), as predicted in the energy-consumption model.²⁴ We attributed this period lengthening to a harder-toactivate Cdk1 requiring more cyclin to reach the same Cdk1 threshold for NEB (Figure 4C, lower branches, asterisks), as the decreased ATP over time favors more unphosphorylated Wee1 (an inhibitor of Cdk1) and less phosphorylated Cdc25 (an activator of Cdk1), causing less Cdk1 activatable for the same cyclin B1 accumulation. Thus, cyclin synthesis alone cannot determine the oscillation speed; it is also subject to the Cdk1 activation threshold that changes with phosphorylation energy. Interestingly, a study in fission yeast also indicated that phosphorylation energy and Cdc13 accumulation synergistically drive Cdc2 activation.³³ For comparable cyclin expression, cells with nuclei showed advanced mitotic entry and shorter period than cells without, although both periods are positively correlated with cyclin peak intensities, also supporting the idea of period lengthening due to more cyclin B1 required to activate Cdk1 (Figures 4D and 4E).

We further explored the impact of compartments on trajectory shapes. In the nucleus-containing droplets, Cdk1 undershot the basal level before a gradual increase with cyclin as compared with being constant throughout interphase in the cytoplasmic droplets, resulting in oblique (blue) versus flat (red) branch #1 in their trajectories (Figure 4F). Comparing orbits of different period lengths, we observed larger cyclin B1 peak values (wider branch #1) for longer cycles (Figure 4G, short, medium, long; Figure S4A for all oscillations). Short cycles have no obvious branch #3. with Cdk1 inactivated almost immediately with cyclin B1 degradation, exhibiting a roughly triangle-shaped orbit. But the longer period droplet not only produced more cyclin but also had more to degrade before Cdk1 started to inactivate (wider branch #3), suggesting that the excessive unbound cyclin B1 was degraded before the bound cyclin B1. Thus, whether the orbit is triangle- or square-shaped depends on the amount of excessive unbound cyclin B1.

Cyclin B1 degradation is scalable

To understand the spatiotemporal dynamics of unbound and bound cyclins, we compared droplets with distinct cyclin expressions. Droplets with over-expressed cyclin B1 formed puncta-like structures that were not seen in the Cdk1 FRET channel (Figures 4H and S4B; Video S4), suggesting these might

⁽H) Representative droplets that expressed cyclin B1-mScarlet-i protein with (+) or without (–) puncta in the cytosolic region (10 ng/μL cyclin B1-mScarlet-i mRNA in bulk extracts). Puncta were observed in a higher cyclin B1 expressed droplet. The degradation time of cyclin B1 was comparable between different conditions. Contraction of cyclin B1 was observed after NEB (yellow frame). The time interval of the montage was 4 min.

⁽I) Cyclin B1 degradation trajectory of droplets with puncta (blue) and without (red). Both droplets showed a similar background intensity after the degradation was complete.

⁽J) The same degradation curves in (I) after normalization.

⁽K) Summary graph of phase-plane trajectories of Cdk1 activity and cyclin B1 in droplets with and without nuclei. See also Figure S4, Videos S3 and S4.

Article



be unbound cyclin. We also observed a large bright structure localized right outside the nucleus (Figure S4C). The small puncta remained in the cytoplasm until NEB when they rapidly aggregated toward the larger structure before being degraded. Similar cyclin structures were also observed in the cytoplasm of starfish oocytes that disappear upon Cdk1 activation.34 Although it is unclear what causes the puncta and their rapid aggregation upon NEB, cyclin B1 is also reported to localize to centrosomes, microtubules, chromatin, and kinetochores, 35,36 and the sudden contraction of these at NEB may be achieved via active microtubule transportation for localization to kinetochores or chromatin DNA. Interestingly, despite the significantly different cyclin expressions among droplets, they degraded within a similar time frame, suggesting a faster degradation process in the droplet with higher expression (Figure 4I). Their relative degradation trends overlapped, exhibiting a comparable half-life (the time taken to reach 50% of the peak) (Figures 4J, S4E, and S4H). This implies that the degradation rate can be scaled with the level of proteins. Studies in different organisms found that mitosis remains constant by insulating itself from the highly variable interphase, thanks to the positive feedback regulation.^{25,37} Our finding of scalable degradation also provides an essential mechanism for droplets with highly variable cyclin expressions and interphase durations to still maintain robust timing of mitosis.

DISCUSSION

We have developed a Cdk1-EV FRET biosensor and synthetic cells to investigate how the eukaryotic segregation of nucleus and cytoplasm affects the Cdk1-network functioning and found it plays an important role in the oscillator robustness and faithful coordination of downstream events. The previously reported Cdk1 FRET biosensor did not work in our cell-free system probably due to the varied sensor domain specificity in different species or poor solubility of this protein expressed in Escherichia coli.38 A modified version by replacing PBD with the FHA2 domain was also reported in HeLa cells but showed substantial cell-to-cell variability in the emission ratio.³⁸ With improved solubility, high signal-to-noise ratio and specificity, and low signal variability demonstrated in our study, Cdk1-EV may apply well to other in vitro and live-cell systems.

We also developed microfluidics to tune cyclin B1 and examined the Cdk1 oscillator properties in reconstituted, spatially different cellular environments, homogenized cytoplasm or discrete nucleocytoplasmic compartments. These single-cell assays were crucial to capture the frequency tunability properties in cytoplasmic droplets, because bulk measurements, by averaging from individuals, may blur the frequency and amplitude quantification.

When cyclin B1 mRNA was not excessive, the nucleocytoplasmic droplets showed shorter periods than cytoplasmic droplets prepared from the same bulk extracts (Figures 3B, 3C, 4D, and 4E). We attributed this accelerated mitotic entry to a nucleus concentrating effect; the concentrated nuclear Cdk1 in turn promotes NEB and activates surrounding cytoplasmic Cdk1 via a trigger wave mechanism, so the nucleus acts as a pacemaker.^{39,40} However, this became ineffective when cyclin mRNA increased beyond a certain level (Figures 3D and 3E) as the oscillation period was changed easily with cyclin B1 in a cytoplasmic droplet but almost unchangeable in a nucleocytoplasmic droplet. Although it requires further investigations, the nucleus-driven robust timing may suggest a buffering mechanism of the compartment, such that when cyclin is dilute in the cytoplasm, nuclear concentrating promotes mitotic entry, but excessive cyclin B1 cannot further expedite mitotic entry if the amount of active cyclin B1-Cdk1 exceeds the nuclear import capacity before NEB. In principle, the time required for DNA replication may also set a limit for how fast the oscillator can run, similar to how DNA is limiting for cell cycle timing found in Drosophila embryos.41 However, we could not detect appreciable DNA replication in our droplets using dUTP or PCNA labeling (Figures S3G and S3H). Our results suggest that segregating a fixed amount of activated cyclin B1-Cdk1 inside the nucleus before NEB may provide spatial insulation from the noisy cytoplasmic environment and help cells resist cyclin fluctuations.

In nucleocytoplasmic droplets, we observed biphasic Cdk1 activation (Figures 3H-3J) that was not reported by the Plk1based Cdk1 FRET sensor in human culture cells, possibly because of the relatively low sensitivity, blurred signal from the sensor shuffling between nucleus and cytoplasm, or systemspecific differences. However, their results support the idea of a gradual activation of Cdk1 to different thresholds to drive the correct temporal order of different mitotic events. 16,42 Other studies in fission yeast and human cells also suggested different Cdk1 levels regulate orderly cell cycle progression, where the level required for mitotic entry is not sufficient for later mitotic progression. 43,44 A similar biphasic Cdk1 activation was also reported during the late syncytial cycles (notably cycle 13) in Drosophila embryos, with the inflection point slightly preceding the completion of DNA replication. 18 The biphasic activation highlights an important effect of the nucleus compartment, as we did not observe the first-phase activation in cytoplasmic droplets, nor did the previous bulk extract studies. Consistent with our findings that the first-phase activation is essential for NEB end, a study on fly embryos also found that although chromosome condensation can occur in the absence of a detectable Cdk1 activity, the prophase exit (NEB end) is a decision point and coincides with Cdk1 activation.4

Cdk subcellular localization was also suggested to enable correct order of different mitotic substrates. 46-48 We show active Cdk1 is initially accumulated inside the nucleus to trigger NEB; after NEB, Cdk1 switches to a higher level to trigger APC activation. Thus, both Cdk1 subcellular localization (via compartmentalization) and distinct phases of activation ensure the robust ordering of downstream events, such that NEB must happen before anaphase onset.

Although the energy depletion theory could explain period lengthening and right-shifted trajectories (Figure 4C), we found extracts with extra cyclins (Figure 2G) or Wee1 inhibition⁴⁹ ran faster for much longer, suggesting the oscillation termination is not caused by extracts running out of energy. Rather, some controlling factors that require future investigations set the cell cycle lifetime in our cell-free system.

We observed a delay between cyclin degradation and Cdk1 sensor inactivation as branch #3 of squared trajectories





(Figures 4G and S4A). Such delay was also observed in mammalian cells and interpreted as a delay in phosphatase activation. 16,50 However, we found these delays are cyclin dependent; the longer the interphase (meaning more cyclin B1 being produced), the longer the delay, and the delay usually disappears for a short cycle, leading to a triangle-shaped loop. Therefore, our interpretation for the delay is the excessive unbound cyclin B1 being degraded before the Cdk1-bound cyclin B1. Consistent with this interpretation, a study in mammalian cells also found that excessive cyclin B1 must be degraded by the time of anaphase onset because even a low level of nondegradable cyclin B1 is sufficient to block the metaphase-anaphase transition.⁵¹ Meiosis of mouse oocytes also preferentially degrades free cyclin B1 because the degradation motif of the Cdk1-bound cyclin B1 is masked by Cdk1, leading to the ordered destruction of the Cdk1-unbound and Cdk1-bound forms of cyclin B1. 17

The mechanism behind the scalable cyclin B1 degradation (Figures 4I, 4J, and S4D-S4I) is unclear and requires further investigation. In a simplified model, we could consider the substrate S (ubiquitinated cyclin B1) interacts with the proteasome following Michaelis-Menten kinetics. For droplets with over-expressed cyclin B1 at a saturating concentration, [S]>>Km, where Km is the Michaelis constant, the initial degradation speed reaches a maximum Vmax, independent of cyclin B1 concentration, leading to a zeroth-order degradation. For droplets with a low cyclin B1 expression, [S] << K_m, the initial degradation rate can be approximated as Vmax [S]/ $K_{\rm m}$, giving the first-order degradation or exponential decay. This might roughly explain the observed scalable degradation, with more cyclin being degraded faster. When plotted on the semi-log scale, the degradation kinetics for higher cyclin expression are curved (zero order) and for low expression are close to linear (first order) (Figures S4D-S4I), consistent with the model expectation.

In conclusion, as illustrated in Figure 4K, our study provided a detailed mapping of single-cell phase-plane trajectories with a unique comparison between the presence and absence of a nucleus. In both cases, cell cycle functions as a typical relaxation oscillator, characteristic of a slow buildup (gradual cyclin synthesis; blue) and an abrupt discharge on a much shorter timescale (switching of Cdk1 in the robust mitotic phase; red), analogous to a capacitor that is charged slowly (stress built up) but discharged rapidly (stress relaxed). The nucleus compartment significantly impacts how Cdk1 responses to cyclin during interphase, changing it from flat to an oblique increase (blue). The cyclin-independent overshoot of Cdk1 activation beyond NEB and undershoot of Cdk1 inactivation after NEF may feature hysteresis and ensure irreversible decision making at mitotic entry and mitotic exit. These features and compartmentalization of Cdk1 together govern the temporal order of its downstream mitotic events.

The findings highlight the importance of cellular compartmentalization and the necessity of cross-checking studies using wellmixed extracts and cells, where the same molecular network may behave differently. Our synthetic cell approach provides a critical tool for uncovering these differences and may be adaptable to exploring the potential functional advantages of other nucleocytoplasmic segregated processes.

Limitations of the study

In this study, we encapsulate cytosolic extracts of frog eggs into fluorosurfactant-stabilized water-in-oil droplets. Unlike culture cells, where reagents can be added in the middle of experiments, we cannot apply reagents such as ATP and kinase inhibitors after encapsulation because these reagents are not diffusible in oil. Our artificial cell system, despite the advantages of quantitative manipulation and analysis of the Cdk1 network and nuclear events, may not capture the complexity of intact live cells and embryos. For example, although we could reconstitute some nuclear events such as NEF and NEB in droplet cells, we could not obtain obvious evidence of DNA replication or the cell cycle checkpoint Chk1 activation, as observed in mammalian cells⁵² and fly embryos. 18

STAR*METHODS

Detailed methods are provided in the online version of this paper and include the following:

- KEY RESOURCES TABLE
- RESOURCE AVAILABILITY
 - Lead contact
 - Material availability
 - Data and code availability
- EXPERIMENTAL MODEL AND SUBJECT DETAILS
 - Egg extract preparation
- **METHOD DETAILS**
 - Plasmids and molecular cloning
- FLUORESCENCE-LABELED REPORTERS
 - Droplet formation
- LIVE CELL IMAGING
- QUANTIFICATION AND STATISTICAL ANALYSIS
 - Image processing
 - Creation of FRET/CFP ratio image stack
 - Data analysis

SUPPLEMENTAL INFORMATION

Supplemental information can be found online at https://doi.org/10.1016/j. celrep.2022.111870.

ACKNOWLEDGMENTS

We thank Michiyuki Matsuda, Dorus Gadella, Xuedong Liu, and Olivier Gavet for providing pPBbsr2-3594nls, pmScarlet-i_C1, pXL-6xHis-CDK1-FRET-JP (originally developed by Jonathon Pines's group), and NLS-mRuby-PCNA constructs, respectively; Yohei Kondo for providing custom the ImageJ macro; and Meng Sun, Shiyuan Wang, Owen Plus, and Minjun Jin for helping on the preparation of microfluidic device and Xenopus egg extracts. This work was supported by grants from the NSF (MCB #1817909; MCB #2218083) and the Alfred P. Sloan Foundation.

AUTHOR CONTRIBUTIONS

G.M. and Q.Y. conceived the project. G.M. performed experiments and analyzed the data. G.M. and Q.Y. wrote the manuscript.

DECLARATION OF INTERESTS

The authors declare no competing interests.

Article

Received: July 28, 2021 Revised: November 15, 2022 Accepted: December 1, 2022 Published: December 27, 2022

REFERENCES

- 1. Murray, A.W. (1991). Cell cycle extracts. Methods Cell Biol. 36, 581-605. https://doi.org/10.1016/S0091-679X(08)60298-8.
- 2. Heald, R., McLoughlin, M., and McKeon, F. (1993). Human wee1 maintains mitotic timing by protecting the nucleus from cytoplasmically activated Cdc2 kinase. Cell 74, 463-474. https://doi.org/10.1016/0092-8674(93)
- 3. Kim, S.Y., and Ferrell, J.E., Jr. (2007). Substrate competition as a source of ultrasensitivity in the inactivation of Wee1. Cell 128, 1133-1145. https:// doi.org/10.1016/j.cell.2007.01.039.
- 4. Sha, W., Moore, J., Chen, K., Lassaletta, A.D., Yi, C.-S., Tyson, J.J., and Sible, J.C. (2003). Hysteresis drives cell-cycle transitions in Xenopus laevis egg extracts. Proc. Natl. Acad. Sci. USA 100, 975-980. https://doi.org/10. 1073/pnas.0235349100.
- 5. Trunnell, N.B., Poon, A.C., Kim, S.Y., and Ferrell, J.E., Jr. (2011). Ultrasensitivity in the regulation of Cdc25C by Cdk1. Mol. Cell 41, 263-274. https:// doi.org/10.1016/j.molcel.2011.01.012.
- 6. Yang, Q., and Ferrell, J.E., Jr. (2013). The Cdk1-APC/C cell cycle oscillator circuit functions as a time-delayed, ultrasensitive switch. Nat. Cell Biol. 15, 519-525. https://doi.org/10.1038/ncb2737.
- 7. Ferrell, J.E., Jr., Tsai, T.Y.-C., and Yang, Q. (2011). Modeling the cell cycle: why do certain circuits oscillate? Cell 144, 874-885. https://doi.org/10. 1016/i.cell.2011.03.006.
- 8. Hahn, H.S., Nitzan, A., Ortoleva, P., and Ross, J. (1974). Threshold excitations, relaxation oscillations, and effect of noise in an enzyme reaction. Proc. Natl. Acad. Sci. USA 71, 4067-4071. https://doi.org/10.1073/pnas.
- 9. Han, Z., Yang, L., MacLellan, W.R., Weiss, J.N., and Qu, Z. (2005). Hysteresis and cell cycle transitions: how crucial is it? Biophys. J. 88, 1626-1634. https://doi.org/10.1529/biophysj.104.053066.
- 10. Li, Z., Liu, S., and Yang, Q. (2017). Incoherent inputs enhance the robustness of biological oscillators. Cell Syst. 5, 72-81.e4. https://doi.org/10.
- 11. Pomerening, J.R., Kim, S.Y., and Ferrell, J.E., Jr. (2005). Systems-level dissection of the cell-cycle oscillator; bypassing positive feedback produces damped oscillations. Cell 122, 565-578. https://doi.org/10.1016/j. cell.2005.06.016.
- 12. Tsai, T.Y.-C., Choi, Y.S., Ma, W., Pomerening, J.R., Tang, C., and Ferrell, J.E., Jr. (2008). Robust, tunable biological oscillations from interlinked positive and negative feedback loops. Science 321, 126-129. https:// doi.org/10.1126/science.1156951.
- 13. Goodwin, B.C. (1966). An entrainment model for timed enzyme syntheses in bacteria. Nature 209, 479-481. https://doi.org/10.1038/209479a0.
- 14. Santos, S.D.M., Wollman, R., Meyer, T., and Ferrell, J.E. (2012). Spatial positive feedback at the onset of mitosis. Cell 149, 1500-1513. https:// doi.org/10.1016/j.cell.2012.05.028.
- 15. Gavet, O., and Pines, J. (2010). Activation of cyclin B1-Cdk1 synchronizes events in the nucleus and the cytoplasm at mitosis. J. Cell Biol. 189, 247-259, https://doi.org/10.1083/jcb.200909144.
- 16. Gavet, O., and Pines, J. (2010). Progressive activation of CyclinB1-Cdk1 coordinates entry to mitosis. Dev. Cell 18, 533-543. https://doi.org/10. 1016/j.devcel.2010.02.013.
- 17. Levasseur, M.D., Thomas, C., Davies, O.R., Higgins, J.M.G., and Madgwick, S. (2019). Aneuploidy in oocytes is prevented by sustained CDK1 activity through degron masking in cyclin B1. Dev. Cell 48, 672-684.e5. https://doi.org/10.1016/j.devcel.2019.01.008.

- 18. Deneke, V.E., Melbinger, A., Vergassola, M., and Di Talia, S. (2016). Waves of Cdk1 activity in S phase synchronize the cell cycle in Drosophila embryos. Dev. Cell 38, 399-412. https://doi.org/10.1016/j.devcel.2016. 07.023.
- 19. Harvey, C.D., Ehrhardt, A.G., Cellurale, C., Zhong, H., Yasuda, R., Davis, R.J., and Svoboda, K. (2008). A genetically encoded fluorescent sensor of ERK activity. Proc. Natl. Acad. Sci. USA 105, 19264-19269. https:// doi.org/10.1073/pnas.0804598105.
- 20. Komatsu, N., Aoki, K., Yamada, M., Yukinaga, H., Fujita, Y., Kamioka, Y., and Matsuda, M. (2011). Development of an optimized backbone of FRET biosensors for kinases and GTPases. Mol. Biol. Cell 22, 4647-4656. https://doi.org/10.1091/mbc.E11-01-0072.
- 21. Aoki, K., Kumagai, Y., Sakurai, A., Komatsu, N., Fujita, Y., Shionyu, C., and Matsuda, M. (2013). Stochastic ERK activation induced by noise and cellto-cell propagation regulates cell density-dependent proliferation. Mol. Cell 52, 529-540. https://doi.org/10.1016/j.molcel.2013.09.015.
- 22. Bonnet, J., Mayonove, P., and Morris, M.C. (2008). Differential phosphorylation of Cdc25C phosphatase in mitosis. Biochem. Biophys. Res. Commun. 370, 483-488. https://doi.org/10.1016/j.bbrc.2008.03.117.
- 23. Franckhauser, C., Mamaeva, D., Heron-Milhavet, L., Fernandez, A., and Lamb, N.J.C. (2010). Distinct pools of cdc25C are phosphorylated on specific TP sites and differentially localized in human mitotic cells. PLoS One 5, e11798. https://doi.org/10.1371/journal.pone.0011798.
- 24. Guan, Y., Li, Z., Wang, S., Barnes, P.M., Liu, X., Xu, H., Jin, M., Liu, A.P., and Yang, Q. (2018). A robust and tunable mitotic oscillator in artificial cells. Elife 7, e33549. https://doi.org/10.7554/eLife.33549.
- 25. Sun, M., Li, Z., Wang, S., Maryu, G., and Yang, Q. (2019). Building dynamic cellular machineries in droplet-based artificial cells with single-droplet tracking and analysis. Anal. Chem. 91, 9813-9818. https://doi.org/10. 1021/acs.analchem.9b01481.
- 26. Guan, Y., Wang, S., Jin, M., Xu, H., and Yang, Q. (2018). Reconstitution of cell-cycle oscillations in microemulsions of cell-free Xenopus egg extracts. J. Vis. Exp. 139, e58240. https://doi.org/10.3791/58240.
- 27. Zhang, W., and Liu, H.T. (2002). MAPK signal pathways in the regulation of cell proliferation in mammalian cells. Cell Res. 12, 9-18. https://doi.org/10. 1038/si.cr.7290105
- 28. Albeck, J.G., Mills, G.B., and Brugge, J.S. (2013). Frequency-modulated pulses of ERK activity transmit quantitative proliferation signals. Mol. Cell 49, 249-261. https://doi.org/10.1016/j.molcel.2012.11.002.
- 29. Li, Z., Wang, S., Sun, M., Jin, M., Khain, D., and Yang, Q. (2021). High-resolution mapping of the period landscape reveals polymorphism in cell cycle frequency tuning. Preprint at bioRxiv. https://doi.org/10.1101/2021.05.
- 30. Weitz, M., Kim, J., Kapsner, K., Winfree, E., Franco, E., and Simmel, F.C. (2014). Diversity in the dynamical behaviour of a compartmentalized programmable biochemical oscillator. Nat. Chem. 6, 295-302. https://doi. ora/10.1038/nchem.1869.
- 31. Cao, Y., Wang, H., Ouyang, Q., and Tu, Y. (2015). The free energy cost of accurate biochemical oscillations. Nat. Phys. 11, 772-778. https://doi.org/ 10.1038/nphys3412.
- 32. Novak, B., Csikasz-Nagy, A., Gyorffy, B., Chen, K., and Tyson, J.J. (1998). Mathematical model of the fission yeast cell cycle with checkpoint controls at the G1/S, G2/M and metaphase/anaphase transitions. Biophys. Chem. 72, 185-200. https://doi.org/10.1016/s0301-4622(98)00133-1.
- 33. Wang, T., Zhao, J., Ouyang, Q., Qian, H., Fu, Y.V., and Li, F. (2016). Phosphorylation energy and nonlinear kinetics as key determinants for G2/M transition in fission yeast cell cycle. Preprint at bioRxiv. https://doi.org/
- 34. Terasaki, M., Okumura, E.-I., Hinkle, B., and Kishimoto, T. (2003). Localization and dynamics of Cdc2-cyclin B during meiotic reinitiation in starfish oocytes. Mol. Biol. Cell 14, 4685-4694. https://doi.org/10.1091/mbc.e03-04-0249.





- 35. Bentley, A.M., Normand, G., Hoyt, J., and King, R.W. (2007). Distinct sequence elements of cyclin B1 promote localization to chromatin, centrosomes, and kinetochores during mitosis. Mol. Biol. Cell 18, 4847-4858. https://doi.org/10.1091/mbc.e06-06-0539.
- 36. Chen, Q., Zhang, X., Jiang, Q., Clarke, P.R., and Zhang, C. (2008). Cyclin B1 is localized to unattached kinetochores and contributes to efficient microtubule attachment and proper chromosome alignment during mitosis. Cell Res. 18, 268-280. https://doi.org/10.1038/cr.2008.11.
- 37. Araujo, A.R., Gelens, L., Sheriff, R.S.M., and Santos, S.D.M. (2016). Positive feedback keeps duration of mitosis temporally insulated from upstream cell-cycle events. Mol. Cell 64, 362-375. https://doi.org/10.1016/ j.molcel.2016.09.018.
- 38. Belal, A.S.F., Sell, B.R., Hoi, H., Davidson, M.W., and Campbell, R.E. (2014). Optimization of a genetically encoded biosensor for cyclin B1-cyclin dependent kinase 1. Mol. Biosyst. 10, 191-195. https://doi.org/10. 1039/c3mb70402e.
- 39. Afanzar, O., Buss, G.K., Stearns, T., and Ferrell, J.E., Jr. (2020). The nucleus serves as the pacemaker for the cell cycle. Elife 9, e59989. https:// doi.ora/10.7554/eLife.59989.
- 40. Nolet, F.E., Vandervelde, A., Vanderbeke, A., Piñeros, L., Chang, J.B., and Gelens, L. (2020). Nuclei determine the spatial origin of mitotic waves. Elife 9, e52868. https://doi.org/10.7554/eLife.52868.
- 41. Farrell, J.A., and O'Farrell, P.H. (2014). From egg to gastrula: how the cell cycle is remodeled during the Drosophila mid-blastula transition. Annu. Rev. Genet. 48, 269-294. https://doi.org/10.1146/annurev-genet-111 212-133531.
- 42. Lindqvist, A. (2010). Cyclin B-Cdk1 activates its own pump to get into the nucleus. J. Cell Biol. 189, 197-199. https://doi.org/10.1083/jcb.201 003032.
- 43. Stern, B., and Nurse, P. (1996). A quantitative model for the cdc2 control of S phase and mitosis in fission yeast. Trends Genet. 12, 345-350. https:// doi.org/10.1016/S0168-9525(96)80016-3.
- 44. Lindqvist, A., van Zon, W., Karlsson Rosenthal, C., and Wolthuis, R.M.F. (2007). Cyclin B1-Cdk1 activation continues after centrosome separation to control mitotic progression. PLoS Biol. 5, e123. https://doi.org/10.1371/ journal.pbio.0050123.
- 45. Falahati, H., Hur, W., Di Talia, S., and Wieschaus, E. (2021). Temperature-Induced uncoupling of cell cycle regulators. Dev. Biol. 470, 147-153. https://doi.org/10.1016/j.ydbio.2020.11.010.

- 46. Basu, S., Roberts, E.L., Jones, A.W., Swaffer, M.P., Snijders, A.P., and Nurse, P. (2020). The hydrophobic patch directs cyclin B to centrosomes to promote global CDK phosphorylation at mitosis. Curr. Biol. 30, 883-892.e4. https://doi.org/10.1016/j.cub.2019.12.053.
- 47. Moore, J.D., Kirk, J.A., and Hunt, T. (2003). Unmasking the S-phasepromoting potential of cyclin B1. Science 300, 987-990. https://doi.org/ 10.1126/science.1081418.
- 48. Swaffer, M.P., Jones, A.W., Flynn, H.R., Snijders, A.P., and Nurse, P. (2016). CDK substrate phosphorylation and ordering the cell cycle. Cell 167, 1750-1761.e16. https://doi.org/10.1016/j.cell.2016.11.034.
- 49. Jin, M., Tavella, F., Wang, S., and Yang, Q. (2022). In vitro cell cycle oscillations exhibit a robust and hysteretic response to changes in cytoplasmic density. Proc. Natl. Acad. Sci. USA 119, e2109547119. https://doi.org/10. 1073/pnas 2109547119.
- 50. Deneke, V.E., Puliafito, A., Krueger, D., Narla, A.V., De Simone, A., Primo, L., Vergassola, M., De Renzis, S., and Di Talia, S. (2019). Self-organized nuclear positioning synchronizes the cell cycle in Drosophila embryos. Cell 177, 925-941.e17. https://doi.org/10.1016/j.cell.2019.03.007.
- 51. Chang, D.C., Xu, N., and Luo, K.Q. (2003). Degradation of cyclin B is required for the onset of anaphase in Mammalian cells. J. Biol. Chem. 278, 37865-37873. https://doi.org/10.1074/jbc.M306376200.
- 52. Lebrec, V., Poteau, M., Morretton, J.-P., and Gavet, O. (2022). Chk1 dynamics in G2 phase upon replication stress predict daughter cell outcome. Dev. Cell 57, 638-653.e5. https://doi.org/10.1016/j.devcel.2022.02.013.
- 53. Schindelin, J., Arganda-Carreras, I., Frise, E., Kaynig, V., Longair, M., Pietzsch, T., Preibisch, S., Rueden, C., Saalfeld, S., Schmid, B., et al. (2012). Fiji: an open-source platform for biological-image analysis. Nat. Methods 9, 676-682. https://doi.org/10.1038/nmeth.2019.
- 54. Edelstein, A.D., Tsuchida, M.A., Amodaj, N., Pinkard, H., Vale, R.D., and Stuurman, N. (2014). Advanced methods of microscope control using μManager software. J. Biol. Methods 1, e10. https://doi.org/10.14440/ jbm.2014.36.
- 55. Edelstein, A., Amodaj, N., Hoover, K., Vale, R., and Stuurman, N. (2010). Computer control of microscopes using µManager. Curr. Protoc. Mol. Biol. Chapter 14, Unit14.20. https://doi.org/10.1002/0471142727. mb1420s92.

Cell Reports Article



STAR***METHODS**

KEY RESOURCES TABLE

REAGENT or RESOURCE	SOURCE	IDENTIFIER
Bacterial and virus strains		
E.coli BL21(DE3)	New England BioLabs	C2527H
E.coli DH5α	New England BioLabs	C2987H
Chemicals, peptides, and recombinant proteins		
KOD one	TOYOBO	KMM-101
Ligation High ver.2	TOYOBO	LGK-201
Calcium ionophore A23187	Sigma-Aldrich	C7522
Chymostatin	Sigma-Aldrich	C7268
Cytochalasin B	MP Biomedicals	2195119
Leupeptin	Sigma-Aldrich	L2023
Pepstatin A	Sigma-Aldrich	P5318
His60 Ni Superflow Resin	Takara bio	635660
IPTG	Invitrogen	15529019
Mini-PROTEAN® TGX TM Precast Gels	BIO-RAD	4561096
EZBlue TM Gel Staining Reagent	Sigma-Aldrich	G1041
2 weight % 008-FluoroSurfactant in HFE7500	Ran Biotechnologies	008-FluoroSurfactant-2wtH-50G
Mineral oil	Macron Fine Chemicals	MK635704
Human Chorionic Gonadotropin	MP Biomedicals	2198591
Trichloro(1H,1H,2H,2H- perfluorooctyl)silane	Sigma-Aldrich	448931
Critical commercial assays		
QIAquick Gel Extraction Kit	QIAGEN	28706
QIAprep Spin Miniprep Kit	QIAGEN	27106
Poly-Prep Chromatography Columns	BIO-RAD	7311550
Amicon® Ultra-4 Centrifugal Filter Unit (10 kDa)	Millipore	UFC801024
mMESSAGE mMACHINE SP6 Transcription Kit	Ambion	AM1340
RNeasy Micro Kit	QIAGEN	74004
Masterflex TransferTubing	ColeParmer	EW-06417-11
WillCo-dish® Glass Bottom dishes	WillCo Wells	GWST-5040
Rectangle MiniatureHollow Glass Tubing	VitroCom	5012
Experimental models: Organisms/strains		
Xenopus laevis adult female	NASCO	https://www.enasco.com/c/ Education-Supplies/Xenopus-Frogs
Xenopus laevis adult male	NASCO	https://www.enasco.com/c/ Education-Supplies/Xenopus-Frogs
Xenopus laevis egg	Xenopus1	N/A
Oligonucleotides		
Morpholino anti-Xenopus-CyclinB1 (ccnb1_a): ACATTTTCCC AAAACCGACAACTGG	Gene Tools, LLC	custom order
Morpholino anti-Xenopus-CyclinB1 (ccnb1_b): ACATTTCTCAA GCGCAAACCTGCA	Gene Tools, LLC	custom order

(Continued on next page)





Continued		
REAGENT or RESOURCE	SOURCE	IDENTIFIER
Morpholino anti-Xenopus-CyclinB2 (ccnb2_l): AATTGCAGCCC GACGAGTAGCCAT	Gene Tools, LLC	custom order
Morpholino anti-Xenopus-CyclinB2 (ccnb2_s): CGACGAGTAGCC ATCTCCGGTAAAA	Gene Tools, LLC	custom order
Recombinant DNA		
pXL-6xHis-CDK1-FRET-JP	Gift from Dr. Xuedong Liu	Gavet and Pines, 2010 ¹⁶
pET21a-CDK1-FRET-JP-NLS	This study	N/A
pET21a-CDK1-FRET-JP-NLS-EV	This study	N/A
oPBbsr2-3594nls	Gift from Dr. Michiyuki Matsuda	Komatsu et al., 2011 ²⁰
pET21a-Cdk1-EV	This study	N/A
pET21a-Cdk1-EV-TAmut	This study	N/A
pCS2+-CyclinB-Katushka	This study	N/A
oCS2+-CyclinB-mScarlet-i	This study	N/A
pET21a-NLS-mRuby-PCNA	This study	N/A
pET45b-EBFP2	This study	N/A
pET45b-NLS-mCherry-NLS	This study	N/A
Software and algorithms		
Fiji	Schindelin et al., 2012 ⁵³	https://imagej.net/Fiji
MATLAB 2019b, 2020b	Mathworks	N/A
Custom ImageJ macro for IMD	Dr. Yohei Kondo	N/A
Elveflow Smart Interface	Elveflow, Paris, France	https://www.elveflow.com/microfluidic-products/microfluidics-software/
Micro-Manager v1.4.23	Edelstein et al., 2010, 2014 ^{54,55}	https://micro-manager.org/

RESOURCE AVAILABILITY

Lead contact

Further information and requests for resources and reagents should be directed to and will be fulfilled by the lead contact, Qiong Yang (qiongy@umich.edu).

Material availability

Plasmids generated in this study can be obtained through the lead contact.

Data and code availability

Original raw imaging data and analyzed MATLAB data files are stored at the lab and will be shared by the lead contact upon request. Original MATLAB codes for droplet analysis are deposited on GitHub. Codes are available from "Zenodo: https://zenodo.org/ badge/latestdoi/568916700".

Any additional information required to reanalyze the data reported in this paper is available from the lead contact upon request.

EXPERIMENTAL MODEL AND SUBJECT DETAILS

Egg extract preparation

Cycling extracts were prepared with freshly squeezed eggs from Xenopus laevis. The squeezed eggs were activated with calcium ionophore A23187 (200 ng/μL) (Sigma-Aldrich) rather than an electric shock.^{1,24} The activated eggs were packed in thin centrifugation tubes before two-step centrifugation at a speed of 20,000 x g to extract the cytosolic materials. Freshly prepared cytosolic extracts were mixed with extract buffer, demembranated sperm chromatin, energy mix, purified proteins, and other reagents for specific experiments. In all experiments, the amount of extract buffer was adjusted when mixing multiple reagents, so the egg extract always accounted for 70% of the total volume. The sperm chromatin DNA was recovered from the testes postmortem. After homogenization and demembranation, it is stored with nuclear preparation buffer containing 0.3% BSA and 30% (w/v) glycerol at -80°C until the experiment.1

Article



METHOD DETAILS

Plasmids and molecular cloning

For the cloning and expression of recombinant protein in E.coli, the pET system was employed as a backbone vector (Novagen). The cDNA of NLS-mCherry-NLS and EBFP2 were amplified by PCR and inserted into the pET-45b vector plasmid with restriction enzymes. EKAREV was a gift from Dr. Michiyuki Matsuda through Addgene (Addgene, Cambridge, MA). All FRET biosensors in this study were developed by modification of this biosensor. Therefore, all FRET biosensors were composed of the same elements except for the sensor domain, ligand domain, and linker length. The sensor domain of Cdk1-EV and TA mutant was replaced by the linker ligation method. To utilize the same fluorophores, NLS, and affinity tag, cDNA of sensor domain and ligand domain of existing Plk1-cyclin B1-based Cdk1 sensor was amplified by PCR and introduced into the EKAREV plasmid with restriction enzymes. The coding region of the FRET biosensor in those plasmids was transferred into a pET-21a vector that has a C-terminal 6x His-tag by restriction enzymes.

For mRNA purification by in vitro transcription, the pCS2+ plasmid that has an SP6 promoter region was used as a backbone vector. cDNA of Katushka and mScarlet-i were amplified by PCR and replaced with the YFP protein region of pCS2-CyclinB-YFP that we used before.²⁴ pmScarlet-i_C1 was a gift from Dr. Dorus Gadella through Addgene.

FLUORESCENCE-LABELED REPORTERS

NLS-mCherry-NLS protein, FRET biosensors, and EBFP2 protein were expressed in BL21 (DE3) competent cells (New England Biolabs) that were induced by 0.4 mM IPTG (Invitrogen) overnight at 18°C. After cells were corrected by centrifugation, they were suspended by ice-cold lysis buffer (25 mM Na₂HPO₄, 25 mM NaH₂PO₄, 300 mM NaCl, 20 mM Imidazole, 1 mg/mL Lysozyme, 1 mM PMSF) and then incubated in a cold room for an hour. Cells were also broken down to release protein through sonication (Branson). Sonication condition is as follows, on ice, duty cycle: 50%, output control: 4, on:30 s off:30 s, and 6 cycles. His60 Ni Superflow Resin (TakaraBio) and Poly-Prep Chromatography Columns were equilibrated by a wash buffer (25 mM Na₂HPO₄, 25 mM NaH₂PO₄, 300 mM NaCl, 20 mM Imidazole) beforehand. Target proteins were incubated overnight at 4°C and eluted with a 4 mL elution buffer (25 mM Na₂HPO₄, 25 mM NaH₂PO₄, 300 mM NaCl, 300 mM Imidazole) after three times wash by wash buffer. All purified proteins were filtered and concentrated by Amicon Ultra-4 10kDa cutoff (Millipore). The quality of purified protein was checked by CBB staining with EZBlue Gel Staining Reagent (Sigma-Aldrich), and their concentration was measured by the Bradford method with a spectrometer (DeNovix). The purified proteins were aliquoted, flash-frozen, and stored at -80°C until use.

All mRNAs were transcribed in vitro and purified using mMESSAGE mMACHINE SP6 Transcription Kit (Ambion) and RNeasy Micro Kit (QIAGEN). mRNA concentration was measured by a spectrometer.

Droplet formation

Fresh egg cycling extract was mixed with a surfactant on a PDMS chamber that was designed in the previous study to form droplets. 25 2% 008-FluoroSurfactant in HFE7500 (Ran Biotechnologies, Inc.) was used as the oil phase for microfluidics. The oil and aqueous phase were driven with Elveflow OB1 multi-channel flow controller (Elveflow) and went through microbore PTFE tubings (ColeParmer) from vials to a PDMS device. For the single-channel droplet formation, the air pressure of the aqueous phase is 1.5 psi, and the oil phase is 2.0 psi. The air pressure of the aqueous phase was controlled between 0.05 psi to 1.5 psi in the reverse phase for two-channel tuning to yield droplets with different concentrations of morpholino in a wide set continuous range.

This flow pump was controlled by Elveflow Software Interface. When droplets were generated and loaded into glass tubes that were pre-coated with trichloro (1H,1H,2H,2H-perfluorooctyl) silane, the tubes were immersed in a glass-bottom dish (WillCo Wells) filled with mineral oil (Macron Fine Chemicals) to prevent sample evaporations.

LIVE CELL IMAGING

Imaging was performed with an inverted microscope IX83 (Olympus) equipped with a UPlanSApo 4x/0.16 objective lens (Olympus), an ORCA-Flash4.0 V3Digital CMOS camera (Hamamatsu Photonics), X-Cite Xylis Broad Spectrum LED Illumination System (Exelitas Technologies Corp.), and a motorized XY stage (Prior Scientific Inc.) at room temperature. The microscope was controlled by Micro-Manager software. 54,55 Time-lapse images were recorded in bright-field and multiple fluorescence channels for up to 2 days at a time interval of 3-6 min.

QUANTIFICATION AND STATISTICAL ANALYSIS

Image processing

Image processing for droplet-based images was performed using custom MATLAB (MathWorks) scripts developed in a previous study.²⁵ Bright-field images were used for the segmentation and tracking of individual droplets. Fluorescent images of nuclear markers were used to define cellular compartments such as nuclear and cytoplasm regions. The standard deviation of fluorescent intensity, skewness of intensity histogram, and multiple thresholds were calculated in every time point and every droplet (Figure S3A).





Based on standard deviation value and skewness, a certain threshold for the Otsu method was applied for nuclear segmentation. Based on segmentation results, we calculated the average ratio value of the cytosolic and nuclear region intensities, which we used to define the timepoints for NEF, NEB Start, and NEB End (Figures 3F, S3B, and S3C). Mean intensities from all fluorescent channels were calculated for each subcellular region of tracked droplets to obtain time course data. In the mitotic phase, the nuclear region and cytosolic region had the same area due to nuclear disappearance.

Creation of FRET/CFP ratio image stack

To generate colored FRET/CFP ratio images shown in figures, image stacks of background-subtracted CFP and FRET images were created with custom Fiji⁵³ macro. After the creation of the FRET/CFP ratio image stack by image calculator function, its values were represented by the intensity-modulated display mode with a custom Fiji macro (gift from Dr. Yohei Kondo).

Data analysis

FRET/CFP emission ratio was calculated by the division between FRET channel intensity and CFP channel intensity. We used a whole area average of a single droplet for all analyses to compare nucleocytoplasmic droplets and cytoplasmic-only droplets. Based on the calculated FRET/CFP ratio value and CFP intensity, peaks and troughs of Cdk1 activity were detected by custom MATLAB scripts. All peak and trough data were screened manually. In this study, from one peak to the next peak is counted as a certain oscillation. Also, the rising period and falling period are defined by peaks and troughs data. With sperm chromatin DNA added condition, some droplets contain a nucleus. We defined the NEF, NEB Start, and NEB End with the cytoplasm/nuclear intensity value ratio of NLS-tagged fluorescent protein. When the cycling extract did not have a nucleus including the mitotic phase, this ratio value must be 1.0 because the nuclear and cytosolic regions had the same area. Therefore, the time point when the ratio value turned to lower than 1.0 was defined as NEF, and the time point when it returned to 1.0 again was defined as the NEB End. To determine the NEB Start, we fitted the last 10 frame data from the Cdk1 activation peak by the logistic function (Equation 1), and the 1st time point that estimated value is larger than minimum asymptote was defined as the NEB Start (Figures S3B and 3C).

$$F(x) = D + \frac{(D - A)}{\left(1 + \frac{(x)^{B}}{C}\right)}$$
 (Equation 1)

For correction of decay trends of FRET/CFP ratio values, linear baselines were estimated in each droplet with its trough values. The amplitude of Cdk1 activity was calculated by subtraction from the raw peak signal to the estimated baseline value at the time point of the peak. The average value of 1st trough values of cytoplasmic-only droplets was used for data normalization for all droplets with both raw signals and corrected signals.

To compare the Cdk1 activation shape with nucleocytoplasmic droplets and cytoplasmic-only droplets, all oscillation data were normalized into 250 data point vectors. A vector that had less than 250 original data points was interpolated by linearly estimated values. On the other hand, extra data points were expunged from more than 250 original data points vectors. Standard deviation values were calculated at each data point to plot a shade with mean value plot.

For boxplot results for period quantification in Figures 3C and 3E, on each box, the central mark indicates the median, and the bottom and top edges of the box indicate the 25th and 75th percentiles, respectively. The whiskers extend to the most extreme data points not considered outliers, and the outliers are plotted individually using the '+' marker symbol. Statistical significance was calculated using two sample t test implemented on MATLAB. Sample number for this calculation (n) is indicated in each figure legend.